

AUTOMATED EXTRACTION OF THE ANTARCTIC COASTLINE USING SNAKES

T. Klinger^a, C. Heipke^b, N. Ott^c, H. W. Schenke^c, M. Ziems^b

^a Geo++ GmbH, Steinriede 8, 30827 Garbsen, Germany – klinger@geopp.de

^b IPI - Institute of Photogrammetry and GeoInformation, Leibniz Universität Hannover, Nienburger Straße 1, Hannover 30167 Germany
– (heipke,ziems)@ipi.uni-hannover.de

^c Dept. of Bathymetry and Geodesy, Alfred Wegener Institute for Polar and Marine Research, Van-Ronzelen Straße 2, 27568 Bremerhaven, Germany – (hans-werner.schenke,norbert.ott)@awi.de

KEY WORDS: Automation, Snakes, Coastline, Antarctica, Landsat, Mapping, Modelling, Updating

ABSTRACT:

In this paper we present an automatic approach for coastline detection from images which is based on parametric active contours (snakes). Snakes require the definition of an energy functional that reflects the underlying coastline model. As for Antarctica, our application domain, the coastline appearance in the used optical images is heterogeneous. Therefore, a single model does not work equally well in all situations. On the basis of an up-to-date Landsat mosaic three different models are formulated that match a large part of the Antarctic coastline, i.e. the transition from ice shelf to water, from ice shelf to sea ice and from rocky terrain to water. For each of the three different cases the energy terms are optimized based on the radiometric properties of the adjacent regions as well as the curvature and the potential change-rate of the coastline itself. A supervised classification for the three classes *ice*, *water* and *rocky terrain* controls the whole process by choosing the most applicable model for a certain image region. With a view to the practical application the developed approach was integrated into a semiautomatic system, where the human operator supervises the optimization process of the contour and interactively corrects the results if the system fails.

1. INTRODUCTION

1.1 Motivation

The location and shape of the Antarctic coastline is sensitive to climatic conditions. Therefore, several works, e.g. (Williams and Hall, 1993 and Scambos et al., 2000) refer to the retreat of the ice sheet as a strong indication of global climate change. New climate models are being generated that lean on the extension of the ice shelves described by the coastline (Bamber and Bindschadler, 1997). The monotone floating of ice shelves and ruptures of ice shelf fronts make the shape of the Antarctic coastline change quickly over time and thus, monitoring requires frequent updates (Vaughan and Doake, 1997). Capturing and updating the coastline is a comprehensive task and is usually carried out by manual exploitation of satellite imagery. In general, image availability for polar regions has increased in recent years due to a larger number of related missions, e.g. Radarsat-1, Landsat ETM+ or MODIS onboard Aqua/Terra. An expert group of the *Scientific Committee on Antarctic Research* (SCAR) works on a homogeneous *international bathymetric chart of the Southern Ocean* (IBCSO), where the most relevant topographic data of Antarctica and the Southern Ocean is collected for storage in a common GIS, the *Southern Ocean GIS* (SOGIS), that includes cartographic representations of the Antarctic coastline (Ott and Schenke, 2007).

Manually mapping and updating the coastline is very time consuming, as with respect to its fractal nature the length of the coastline as detected in modern satellite imagery reaches almost the size of the earth's equator. This is the basic motivation for

trying to automate the task. In the following, we describe a strategy for updating the Antarctic coastline with a reduced manual effort that makes more frequent update cycles possible.

1.2 Related Work

In the last two decades a couple of approaches were developed that automate the coastline extraction based on satellite imagery with respect to the Antarctic context.

Ryan et al. (1991) applied a texture classification to scanned aerial photographs based on a neural network approach. The coastline is defined as the boundary between different homogeneous regions. Templates for the calculation of the neighbourhood information of the selected texture features lead to smoothing the boundaries and thus to a reduced geometric accuracy of the coastline. Liu and Jezek (2004) classify regions adjacent to the coastline based on intensity values in RADARSAT-1 images, which usually provide better contrast than available optical sensors for the Antarctic context. The classification strategy assumes the bimodal character of the SAR image histogram in coastal regions. Locally adaptive contrast ratio thresholds are determined to separate image regions. After the classification step several shape descriptors are employed to generate plausible regions, whose boundaries are the basis for the coastline extraction. This approach proofed its practicability when the complete Antarctic coastline was extracted from a SAR image mosaic of 25 m and 100 m resolution with a relative precision of one pixel.

In contrast to these region-based classification strategies a second group of approaches is based on edge detection. For updating Fischler and Bolles (1981) generate profiles orthogonal to the given line elements. The updated line points are then determined by maximising the gradient along each of the profiles. This strategy provides stable results for low resolution imagery. For the more complex situations in higher resolution imagery with e.g. shadow effects, rifts on the object surface and a structured shape the algorithm fails. In (Lee and Jurkevich, 1990) a coastline is extracted from a Sobel filtered SAR image. Gaps are bridged by extending the extracted edges, a final grouping leads to a solution for the coastline. A major problem of such a strategy is to handle ambiguities during the grouping process.

To overcome the problems of the former approaches Mason and Davenport (1996) presented a hierarchical strategy that combines a region-based classification and an edge-based strategy. In a first step a SAR image of reduced resolution is used to detect an approximate position of the coastline by classification of the adjacent regions. Subsequently, an active contour model (Kass et al. 1987) is applied to find a geometrically accurate solution in the image of original resolution. A further development of this idea is described in (Della Rocca et al., 2004). Here the initial contour is derived from the output of a wavelet operation.

1.3 Data

Images for the present work are taken from the Landsat Image Mosaic of Antarctica LIMA (Bindshadler et al., 2008). This dataset includes more than 1000 single Landsat images re-sampled to a geometric resolution of 240m and combined into a RGB and IRRG mosaic that covers Antarctica up to southern latitude of 82.5°. Additionally, a coastline derived from the MODIS Image Mosaic Of Antarctica MOA is used as approximate position to be refined with the presented approach. This coastline has a geometric accuracy of about 250 m (Scambos et al, 2007), the temporal difference to the LIMA imagery amounts to about 2 years. With respect to LIMA the potential geometric accuracy of the presented approach is assumed to be about one pixel or 240 m.

2. METHOD

From the literature one can conclude that the incorporation of a sufficiently good approximation is of major importance to find an accurate and reliable final solution. Another aspect is that region-based methods that operate more globally provide reliable results while the more locally operating edge-based methods show a better geometric accuracy. We follow the thoughts of Mason and Davenport (1996) and present a method which uses parametric active contours (snakes) as the core algorithm. The required initialisation is derived from the MOA coastline. We make use of optical instead of SAR images and define a new coastline model consisting of three individual and different snake models. For this purpose representative regions on both sides of the initial coastlines are classified so that the appropriate model can be chosen automatically. The related snake algorithm then improves the position of the coastline. A graphical user interface is provided for supervising the extraction. The human operator can accept the result by confirming it with a simple click, alternatively

he can interactively digitise coastline points and thus refine or correct the automatically obtained result.

In the following the underlying model, the strategy for realising the model within a snake algorithm and the graphical user interface are described in detail.

2.1 Model Definition

The spectral and geometric characteristics of the Antarctic coastline in optical imagery are heterogeneous, so that no single model can reflect the different appearances equally well. On the basis of the Landsat mosaic three different models are formulated that match a large part of the Antarctic coastline, i.e. the transition from ice shelf to water, from ice shelf to sea ice and from rocky terrain to water (Figure 1), where “ice shelf” includes grounded as well as floating ice shelf, and “sea-ice” is not older than one year, and is frequently covered by snow, which makes it hard to distinguish it from ice shelf. The fourth model in this row would be the transition from rocky terrain to sea-ice. This model, however, is not regarded further, since it appears only very seldom in the available imagery.

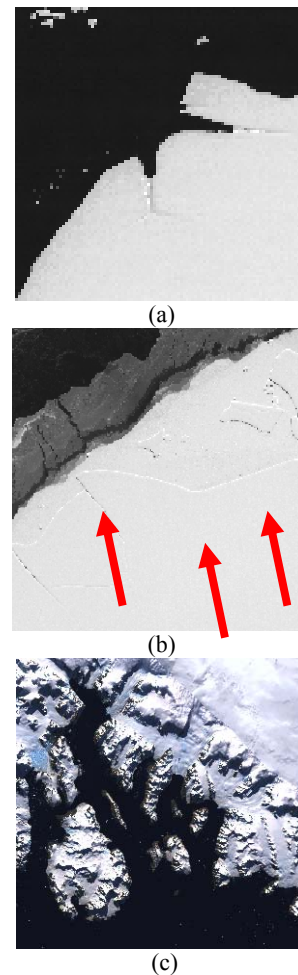


Figure 1: LIMA subsets with instances of the transitions from; a) ice shelf to water; b) ice shelf to sea-ice (the coastline is marked by red arrows); and c) rocky surface to water

The following describes the three models:

Ice shelf to water

- always clear contrast
- largest contrast in the blue channel of LIMA RGB
- shape of the coastline mostly smooth except for rifts
- infrequent preloaded annual ice (ice floes)
- temporal changes of up to 1 km/a (Brunt et al, 2010)
- homogeneous adjacent regions

Ice shelf to sea ice

- small difference in intensity, colour and texture
- change of slope and illumination effects can result in a dark (shadow) or a bright line
- shape of the coastline mostly smooth
- high temporal changes of up to 1 km/a

Rocky terrain to water

- partly low contrast between water and rocky surface
- high contrast between rocks and ice
- static coastline, only inaccuracies of the initialisation are expected
- curvy coastline due to rifts

2.2 Strategy

Pre-processing: Due to the heterogeneous coastline characteristics as well as the immense data volume it is not reasonable to process the complete Antarctic coastline simultaneously. Instead, the Landsat mosaic is segmented into a number of tiles of equal size (here: 460 tiles of 240² km² each), and an active contour is placed over each tile containing a section of the given coastline. The relevant image tiles are automatically selected by a point-in-polygon test with the points of the given coastline as input for the polygon. Hence, our method makes use of open piece-wise linear curves for the coastline detection. The geometric model of the coastline is a polygonal curve supported by the discrete 2D pixel coordinates of the underlying image.

Model Selection: An automated analysis is carried out for each image tile to find the best-matching model. For that purpose the adjacent regions of the expected coastline are classified by a supervised k-nearest-neighbour algorithm based on training samples selected manually for the three classes: ice (ice shelf or sea-ice), water and rocky terrain. For the classification we select two features: the intensity mean and standard deviation. The test segments to be classified are taken from either side of the initial coastline. The segments are generated parallel to its central section, shifted off- and onshore (see Figure 2). The size of the shift is set with respect to the upper bound of the expected maximum offset between the given coastline and its potential current position in the image. Subsequently, the classification results for the segments on either side of the given coastline are combined and from the result, the correct model is selected.

Parameterisation of snakes: Snakes require the definition of an energy functional that reflects the underlying coastline model. For each of the three different models the energy terms and related parameters are optimized based on the radiometric properties of the adjacent regions as well as the curvature and the potential change-rate of the underlying coastal region. Traditionally, a

snake is considered as a curve $v(s) = (x(s), y(s))$ parameterised with the arc length $s \in [0, 1]$, that iteratively moves in the image domain $I(x, y)$ until it minimizes the energy functional of the curve (Kass et al. 1987):

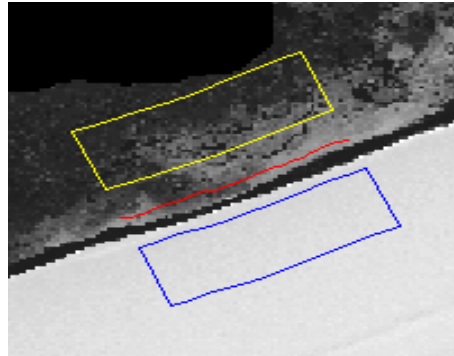


Figure 2: Classification of regions adjacent to the approximate coastline (in red): water (yellow) and ice (blue)

$$E_{snake}^* = \int E_{int}(v(s)) + E_{con}(v(s)) + E_{img}(v(s)) ds \quad (1)$$

The internal energy E_{int} is defined for the description of the shape of the snake and thus varies with every deformation of the curve. Typically the bending and stretching of v are the considered internal snake characteristics, modelled by the first and second derivatives of v with respect to s :

$$E_{int}(v(s, t)) = \frac{1}{2} \cdot [\alpha \cdot |v'(s, t)|^2 + \beta \cdot |v''(s, t)|^2] \quad (2)$$

where E = internal energy
 v', v'' = derivations of v with respect to s
 α = elasticity parameter
 β = rigidity parameter

The elasticity and rigidity parameters act as weighting factors of the first and second order term of Equation 2. The first term controls the length of the snake. Large values for α stretch the coastline more and more but also smooth the effect of local disturbances in the image energy. The second term controls the curvature of the snake. Therefore, β allows to adapt the shape properties of the coastline models, e.g. large values for β lead to a straighter coastline while small values allow a high curvature coastline.

The constraint energy E_{con} and the image energy E_{img} of Equation 1 are considered as context dependent external influences that affect the snake's position, being responsible for iterative movements and deformations. Constraint energy E_{con} can make the snake move toward or away from fixed points or lines. Such points could be of supreme quality, e.g. seed points measured interactively by a human operator, GPS measurements or other in-situ observations. In the current method constraints are not considered but could easily be added in future.

The image energy E_{img} can be considered as a scalar potential energy that is defined for each pixel as a function of the grey levels $I(x, y)$. It hence can be calculated once in advance before starting the iterative optimisation procedure. Principally, the image energy can be defined in various ways. For the present

approach two energy definitions that both attract the snake to edges in the image are selected. The first simply regards the squared magnitude of the gradient image:

$$E_{img}^{STD} = -|\nabla I(x, y)|^2 \quad (3)$$

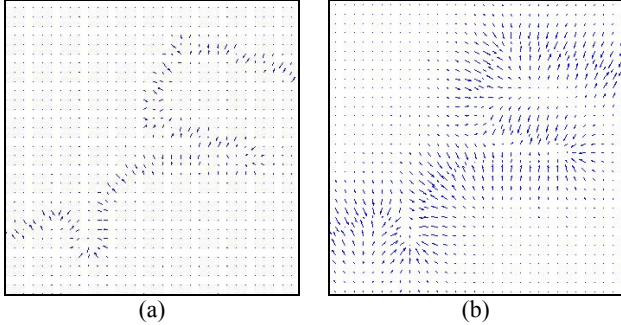


Figure 3: Vector field of image depicted in Figure 1a (transition from shelf ice to water); a) standard vector field with vectors pointing toward the edges; b) GVF field, the snake can be initialized anywhere in the GVF field for being pulled toward an edge

As can be also seen in Figure 3a the range of the image energy field is limited with respect to the width of the template of the gradient operator. As soon as the distance to the initialisation is only slightly higher the calculated energy field does not affect the snake at all. Thus, we make use of a modified energy field E^{GVF} , if the initial coastline is expected to be out of range. Xu and Prince (1997) define that Gradient Vector Flow (GVF) field as a diffusion of the gradient vectors defined in Equation 3. The GVF increases significantly the capture range of the snake and also enables the snake to progress into concave parts of the boundary (Figure 3b). Further adjustment of the image energy term is achieved by model specific pre-processed input image functions, like Median and Sobel filter or HSI transformation. A complete list of the applied pre-processors is given in Table 1 while their effects are displayed in sections 3.1 - 3.3.

In order to minimize the snake energy E^* the related Euler equation must be solved:

$$\alpha \cdot v''(s) - \beta \cdot x''' - \nabla E_{img} = 0 \quad (4)$$

which leads to:

$$v(t) = (A + \gamma \cdot I)^{-1} \cdot [\gamma \cdot v(t-1) - \kappa \cdot f_v(v(t-1))] \quad (5)$$

where

- t = time
- A = design matrix
- γ = step size (viscosity factor)
- I = identity matrix
- κ = weight factor for external energy
- f_v = gradient values from image energy

In Equation 5 the snake is made dynamic by describing v as a function of time. The matrix $A + \gamma I$ is a pentadiagonal banded matrix and γ is a step size that influences the viscosity of the snake. κ denotes the strength of the external energy and f the

gradient values of the image energy (for details of snake optimisation see Kass et al. 1987).

User Interaction: The presented method already considers three different models but obviously unexpected situations can occur nevertheless. To guarantee an optimal quality of the final result the two sub-algorithms *model selection* and *snake algorithm* are supervised by a human operator. To this end a graphical user interface was implemented to monitor the whole process. The graphical user interface consists of two windows in which the initial and the refined data are displayed. It allows manipulating all snake parameters and restarting the process.

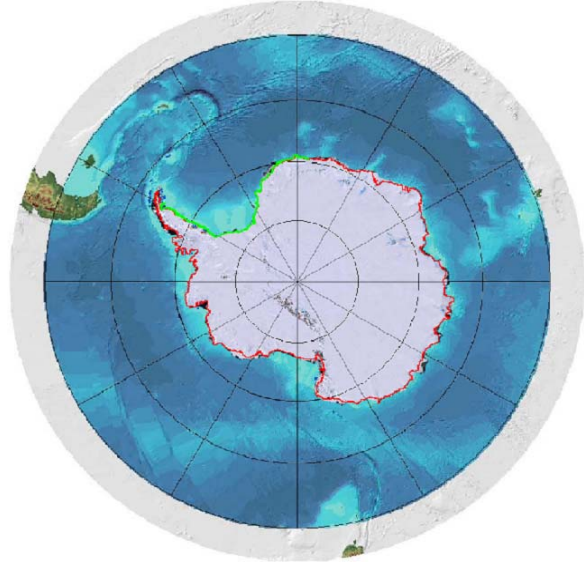


Figure 4: IBCSO with MOA coastline as red curve and processed coastline section as green curve, superimposed to the polar stereographic projection of LIMA and the General Bathymetric Chart of the Oceans (GEBCO) seabed topography.

3. EXPERIMENTS AND RESULTS

Until now, approximately 5000 km or 12% of the Antarctic coastline have been processed with our approach around the Weddell Sea. The part marked in green in Figure 4 illustrates the scope of the experiments. The pre-processing step generated 16 image-tiles of 240 km² each. For each image-tile a coastline model was selected automatically. The applied default snake parameter settings are displayed in Table 1.

The test scenario consists of 8 tiles that show “ice shelf to water” situations, 7 tiles that show “ice shelf to sea ice” and one contains a significant part of a rocky coastline. For all image tiles the automatic model selection results in the best fitted model.

3.1 Ice shelf to water

Figure 5 shows an example of a subset of a LIMA considered as ice shelf to water where the red line in Figure 5a marks the initial MOA coastline. For the displayed example the initial line differs by up to 4 pixels (1km) from the position indicated by the image.

The input image is pre-processed by a Sobel operator, a threshold that filters weak edges like small ice rifts and morphological operators that lead to thin edges. The resulting edge image (Figure 5b) is further processed yielding the GVF field (Figure 5c). The snake optimisation results in the green line, drawn in Figure 5d. We applied the default parameters specified in Table 1: a relatively large value for β and a small value for κ that both lead to a relatively straight coastline. Thus, small rifts and similar structures do not affect the result. The optimisation term is parameterised by a relatively large value for γ (step size) that leads to a fast convergence of the snake (low number of required iterations).

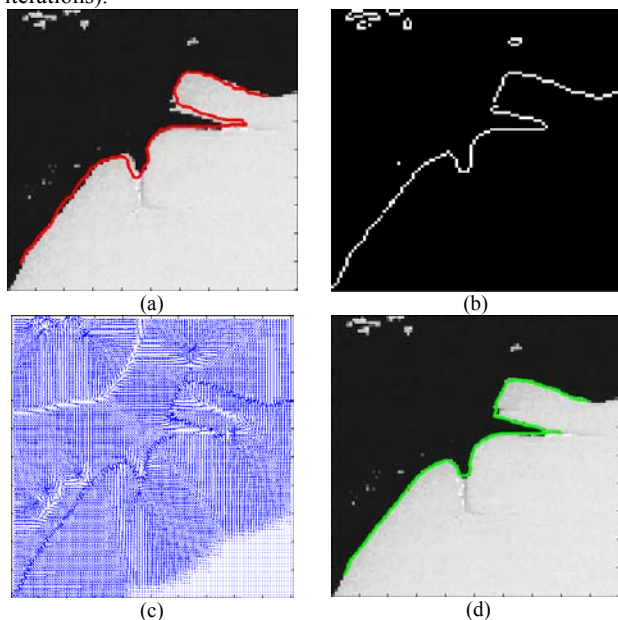


Figure 5: Ice shelf to water model a) a 24*24 km² subset of LIMA showing floating ice shelf next to open water with the corresponding MOA coastline as red curve b) result after edge detection, thresholding and thinning c) GVF field representing the vector force field that affects the snake d) result of the coastline detection (green)

Due to the high intensity contrast between water and shelf ice the refined coastline reflects the image content for the major amount of the tested tiles rather well. Disturbances like preloaded ice floes or structures within the ice-shelf usually do not affect the result. The predefined parameter settings did not need to be adapted while running the test scenario.

3.2 Ice shelf to sea ice

Figure 6 shows a typical constellation of annual ice around an ice shelf on the lower right side of the red marked coastline. The initial coastline in Figure 6a differs by up to 5 pixels (1.25 km) from the image content, the coastline is characterised by a bright and a dark line. The dark line in the lower left results from a shadow of the shelf itself. The bright line results from the directly illuminated shelf. Figure 6b shows the pre-processed image, where a Sobel filter, a threshold and a thinning operation were applied. Here we use a standard vector field as image energy (Figure 6c).

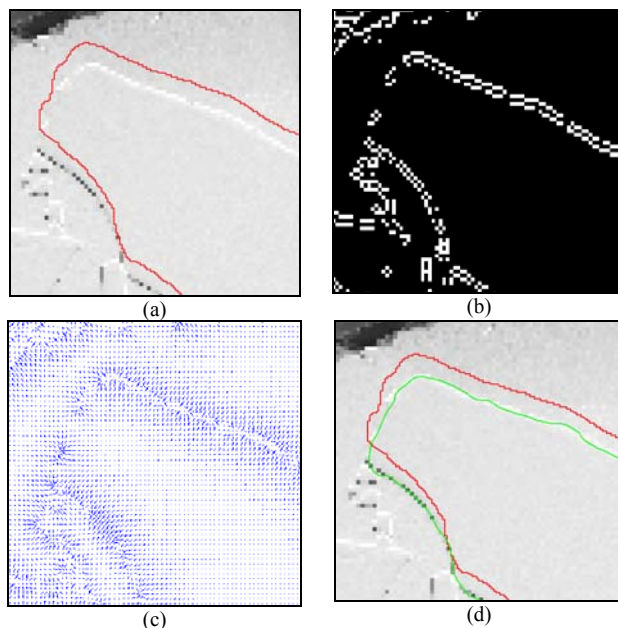


Figure 6: ice shelf to sea-ice model a) a 18*18 km² subset of LIMA showing ice shelf next to sea ice with the corresponding MOA coastline as red curve b) result after edge detection, thresholding and thinning c) standard vector field d) resulting coastline (green)

The main reason for the standard VF is that the offshore water-to-sea ice borderline is potentially very near. Due to its high contrast compared to the targeted coastline the GVF field might therefore lead to a wrong result. The internal energy is parameterised by a large β and κ that result in smaller curvature for the coastline but also strengthen the effect of the image energy compared to the internal energy.

Compared to the ice shelf to water model, ice shelf to sea ice situations often required manual interaction during the test scenario. The changes in the default parameter set (Table 1) are mainly related to the interchange between GVF and standard VF, which was necessary if the initial MOA coastline was too far away.

3.3 Rocky terrain to water

Especially the peak of the Antarctic Peninsula is characterised by rocky terrain, as can be seen in Figure 7. For the major part of the rocky terrain the initial MOA coastline lies nearby the image content. Nevertheless, the example in Figure 7a shows partly differences of up to 3 pixels (0.75 km), which could be removed by our method (Figure 7d). As the dark rocks only show a weak contrast to the water in the intensity channel we used the saturation channel of the HSI transformed RGB image instead. In Figure 7b the blue water shows a relatively large saturation while rocks and ice show nearly no colour. The saturation image is further processed by Median and, Sobel filter, thresholding and thinning. Due to the small difference between the initial MOA coastline and the image content a standard vector field (Figure 7c) and small values for γ are sufficient. Due to its potentially high curvature we selected a small value for β .

For the major part the resulting coastline equals the initial MOA coastline, only for a minor part some enhancement could be achieved as shown in (Figure 7).

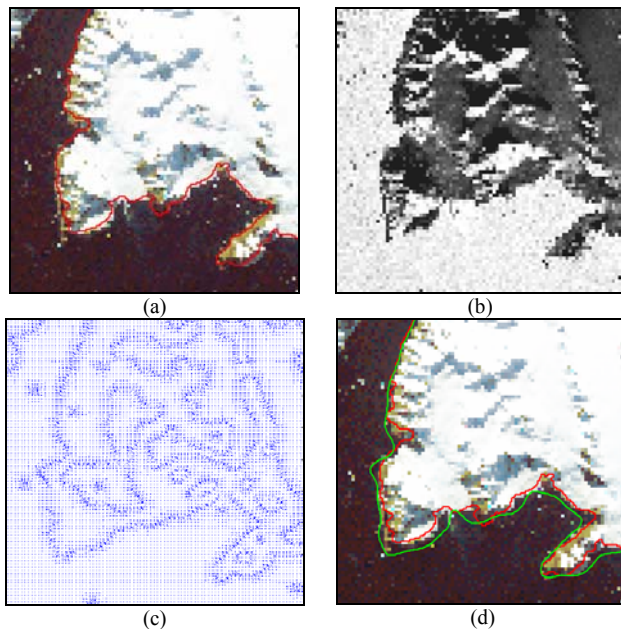


Figure 7. rocky-terrain to water model a) a 22*22 km² subset of LIMA showing the transition of rocky terrain to water with the corresponding MOA coastline as red curve b) saturation channel c) standard vector field d) result of the coastline detection (green)

3.4 Quantitative evaluation of the results

For the evaluation of the proposed method, a reference dataset was extracted manually from the LIMA imagery for the coastline segment, highlighted in Figure 4.

For the processed coastline quality criteria as correctness and completeness are calculated in accordance with Heipke et al. (1997) using the reference dataset. For that purpose, the required geometrical accuracy for the processed coastline was set to 240 m and the geometrical accuracy of the reference dataset was estimated to be 120 m. According to these values the quality criteria result in a completeness of 86.8 % and a correctness ratio of 84.0 %. In other words 13.2 % of the manual reference cannot be detected by the approach (false negative) and 16.0 % of the obtained result is detected wrongly (false positives). Thus, a manual post processing is still necessary, but the manual efforts are drastically reduced compared to a complete manual digitisation of the coastline.

The main issue leading to wrong solutions are adjacent local minima in the image energy related to ambiguities in the edge image. Additionally, different models might occur within one image tile so that there is actually no guaranty that the detected snake model fits equally well for the entire scene.

4. CONCLUSIONS

The developed approach is capable of extracting the Antarctic coastline in its most specific formations with a high degree of automation. Satisfying quality values can be achieved if the set of free parameters is optimised for each employed model. The implemented GUI provides a practical solution to adapt the most sensitive parameters during the process. Thus, the method can be utilized as a tool for an automated change analysis for climate studies or similar tasks.

To increase the correctness and completeness ratios, future work will need to consider enhanced model selection in order to prevent different models being present in one tile. For that purpose additional data sources like the Antarctic Digital Database (ADD), which contains coastline and land cover information, that can be utilized to support the classification algorithm.

Principally, the transition of shelf ice to sea ice is considered as the most limiting issue leading to false extractions. We plan to investigate if a replacement of the used edge oriented definition by a line oriented one yields better results.

For the rocky terrain to water model an additional force field that pushes the snake away from the onshore part could be added to prevent the detection of inland edges so that the capture range of the snake can be extended without drawback.

Furthermore a rocky terrain to ice model will be added to the method to cover all potential transitions on the Antarctic continent.

REFERENCES

- Bamber, J.L., and Bindschadler, R.A., 1997. An improved elevation dataset for climate and ice-sheet modelling: validation with satellite imagery. *Ann. Glaciol.*, 25, 439-444.
- Bindschadler, R., Vornberger, P., Fleming, A., Fox, A., Mullins, J., Binnie, D., Paulsen, S.J., Granneman, B., Gorodetzky, D., 2008. The Landsat Image Mosaic of Antarctica. *Remote Sensing of Environment*, Vol. 112, Issue 12, pp. 4214-4226.
- Brunt, K.M., King, M.A., Fricker, H.A., MacAyeal, D.R., 2010. Flow of the Ross Ice Shelf, Antarctica, is modulated by the ocean tide. *Journal of Glaciology*, Vol. 56, No. 195. 157 - 161.
- Della Rocca, M.R., Fiani, M., Fortunato, A., Pistillo, P., 2004. Active Contour Model to Detect Linear Features in Satellite Images. *International Archives of Photogrammetry, Remote Sensing and Spatial Information Sciences*, Vol. 35, part B3, 446-450.
- Fischler, M.A., and Bolles, R.C., 1981. Random sample consensus: a paradigm for model fitting with applications to image analysis and automated cartography. *Communications of the ACM*, v.24 n.6, pp. 381-395.

Heipke, C., Mayer, H., Wiedemann, C., Jamet, O., 1997. Evaluation of automatic road extraction. *Int'l Arch. Photogrammetry Remote Sensing*, XXXII/3-4W2, pp. 151-160.

Kass, M., Witkin, A., and Terzopoulos, D., 1987. Snakes: Active contour models. *Int. Journal of Computer Vision*, 1(4), pp. 321-331.

Lee, J.S., and Jurkevich, I., 1990. Coastline detection and tracing in SAR images. *IEEE Transactions on Geosciences and Remote Sensing*, 28, pp. 662-668.

Liu, H., and Jezek, K.C., 2004. A complete high resolution coastline of Antarctica extracted from orthorectified Radarsat SAR imagery. *Photogrammetric Engineering & Remote Sensing*, 70(5), pp. 605-616.

Mason, D.C., Davenport, I.J., 1996. Accurate and efficient determination of shoreline in ERS-1 SAR images. *IEEE Transactions on Geoscience and Remote Sensing*, 34, pp. 1243-1253.

Ott, N., and Schenke, H.W., 2007. GIS based data compilation of the new International Bathymetric Chart of the Southern Ocean (IBCSO). U.S. Geological Survey and National Academics, USGS Open File Report 2007-1047, Extended Abstract 023, pp 1-4.

Ryan, T.W., Sementilli, P.J., Yuen, P., and Hunt, B.R., 1991. Extraction of shoreline features by neural nets and image processing. *Photogrammetric Engineering & Remote Sensing*, 57, pp. 947-955.

Scambos, T.A., Hulbe, C., Fahnestock, M., Bohlander, J., 2000. The link between climate warming and break-up of ice shelves in the Antarctic Peninsula. *Journal of Glaciology*, Vol. 46, No. 154, pp. 516-530.

Scambos, T.A., Haran, T.M., Fahnestock, M., Painter, T., Bohlander, J., 2007. MODIS-based Mosaic of Antarctica (MOA) datasets: Continent-wide surface morphology and snow grain size. *Remote Sensing of Environment*, 111, pp. 242-257.

Vaughan, D.G., Doake, C.S.M., 1996. Recent atmospheric warming and retreat of ice shelves on the Antarctic Peninsula. *Nature*, 379 (6563), pp. 328-331.

Williams, R.S., Jr., and Hall, D.K., 1993. *Glaciers, Atlas of Satellite Observations Related to Global Change* (R.J. Gurney, J.L. Foster and C.L. Parkinson, editors), Cambridge University Press, Cambridge, United Kingdom, pp. 401-422.

Xu, C., and Prince, J.L., 1997. Gradient Vector Flow: a new external force for snakes. *IEEE Proc. Conf. on Comp. Vis. Patt. Recog. (CVPR '97)*, pp. 66-71.

| Parameter | | Ice shelf to water | Ice shelf to sea ice | Rocky terrain to water |
|--------------------|------------------------|--------------------|----------------------|---|
| Internal Energy: | - α | 0.01 | 0.01 | 0.01 |
| | - β | 0.1 | 0.2 | 0.001 |
| Image Energy: | - image pre-processing | Sobel filter (3*3) | Sobel filter (3*3) | HSI transformation Median filter (5*5) Sobel filter (3*3) |
| | - vector field | GVF | Standard VF | Standard VF |
| Optimization Term: | - γ | 1 | 0.1 | 0.1 |
| | - κ | 1 | 10 | 10 |
| | - iterations | 20 | 40 | 40 |

Table 1. Parameter settings for the different coastline models